atmosphere

MDPI

Article

Stable Emulation of an Entire Suite of Model Physics in a State-of-the-Art GCM using a Neural Network

Alexei Belochitski[1,2,*], Vladimir Krasnopolsky[2]

[1] IMSG; alexei.a.belochitski@noaa.gov
[2] NOAA/NWS/NCEP/EMC; vladimir.krasnopolsky@noaa.gov
* Correspondence: alexei.a.belochitski@noaa.gov
Received: date; Accepted: date; Published: date

Abstract: There has been a lot of recent interest in developing hybrid models that couple deterministic numerical model components to statistical model components derived using machine learning techniques. One approach that we follow in this pilot study is to replace an existing computationally expensive deterministic model component with its fast machine-learning-based emulator, leading to the model speed-up and/or improvement. We developed a shallow neural network-based emulator of a complete suite of atmospheric physics parameterizations in NCEP Global Forecast System (GFS) general circulation model (GCM). The suite emulated by a single NN includes radiative transfer, cloud macro- and micro-physics, shallow and deep convection, boundary layer processes, gravity wave drag, land model, etc. NCEP GFS with the neural network replacing the original suite of atmospheric parameterizations produces stable and realistic medium range weather forecasts for 24 initial conditions spanning all months of 2018. It also remains stable in a year-long AMIP-like experiment and in the run with a quadrupled horizontal resolution. We present preliminary results of parallel runs, evaluating the accuracy and speedup of the resulting hybrid GCM.

Keywords: general circulation model; neural network; model physics, machine learning, emulation, hybrid model

1. Introduction

Machine learning (ML) can be used in parameterization development at least in two different ways: 1) as an emulation technique for accelerating calculation of parameterizations developed previously and 2) for development of new "empirical" parameterizations based on reanalysis/observed data or data simulated by high resolution models. The former approach was followed by several authors [1-7] For example, in [5] highly efficient neural network (NN) emulations of both long– and short-wave radiation parameterizations for a high resolution state-of-the-art short– to medium-range weather forecasting model have been developed. NN was used in [8] to emulate 2D cloud resolving models (CRMs) embedded into columns of a "super-parameterized" general circulation model (GCM). More recently [9], NN has been used to emulate 2D CRM embedded into columns of a "super-parameterized" aqua-planet configuration with prescribed invariant zonally symmetric SST, full diurnal cycle, and no annual cycle , and in [7] deep NN was used to emulate cloud super-parameterization in realistic geography, using training data from the Super Parameterized Community Atmospheric Model (SPCAM5). Illustration of the latter approach are works [10-12] where the authors built an NN-based deep convection parameterizations by up-scaling CRM tendencies to the GCM scales.

Building ML emulation of the entire block of model physics parameterizations or the model physics suite (MPS) in a state-of-the-art GCM is an attractive task: if successful, it could contribute to development of methodology for constructing new ML-based "empirical" parameterizations, in

addition to the speedup of model calculations. This task may be aided by the fact that the full diabatic forcing profiles in atmospheric models are generally smoother than forcing profiles from individual processes, because the latter often balance each other. In [13] problems arising when emulating full model physics using NNs are discussed, and methods addressing some of those problems are developed.

In this study we present preliminary results of our work on emulating a complete suite of model physics parameterizations in NOAA National Centers for Environmental Prediction's (NCEP) Global Forecast System (GFS) GCM, using a shallow NN-based emulator. In Section 2 of this paper we describe the configuration of GFS that was used in the study. In Section 3, the training set design and the NN architecture is presented. In Section 4 the way of coupling the NN physics in hybrid GFS (HGFS) is described. Section 5 presents preliminary results of parallel runs of HGFS (GFS with NN physics) and GFS. In Section 6 the results are discussed, and future work is outlined.

2. NCEP Global Forecast System Configuration

The GFS version 16 is the foundation of NCEP's new production suite slated to become operational in 2021. Dynamical core of the GFS is a finite volume cubed-sphere non-hydrostatic global model (FV^3, [14,15]) with spatial quasi-uniform resolution of C768 (~ 13 km), and 127 fully Lagrangian layers on a hybrid sigma-pressure vertical coordinate. The GFS contains a comprehensive physics suite [16] that includes parameterizations of radiative transfer [17,18], planetary boundary layer processes [19], orographic and convective gravity wave drag [20,21], deep convection [22,23], shallow convection [24,25], and microphysics [26,27]. In addition, effects of time varying carbon dioxide, trace gases, stratospheric and tropospheric aerosols, as well as ozone and H2O photochemistry are included. The Noah Land Surface Model [28] is employed in GFS as a part of the model physics suite (MPS).

Our study is a proof of concept, so we reconfigure the GFS with the goal of substantially reducing the computational resources necessary to perform both model simulations and the NN training, as well as the storage requirements for the model output and data for NN training and validation, without downgrading the level of sophistication of the GCM. To this end, GFS was used in a configuration with the horizontal resolution of C96 (~ 100 km) and vertical resolution of 64 vertical layers. We also used Zhao-Carr microphysics scheme [29] and the K-profile-based PBL parameterization [24]. In this configuration the atmospheric model state, as seen by the physics package, is given by seven prognostic variables: zonal and meridional wind components, temperature, water vapor, total condensate, and ozone mixing ratios, as well as pressure. Only the first six of these variables are modified by physical parameterizations and returned to the dynamical core in the updated form.

However, there is one aspect of the experimental model configuration that makes our version of the model more sophisticated than the standard/operational GFS. In the latter, the radiative transfer parameterizations are invoked less frequently than the rest of model physics because of their computational expense. For example, there is a single radiation call per 8 calls to the rest of the physical parameterizations in the GFS using C96 horizontal resolution. Because the NN emulation of MPS will encompass the entire model physics block, including the radiation, and because it is going to be invoked at the same frequency as the non-radiative physics, we configure the GFS to call radiation as often as the rest of the model physics for the sake of consistency between experimental NN and control configurations. In what follows, a reference to GFS control assumes the version of GFS configured as described in this Section.

3. Training Set Design and NN Architecture

3.1. Training Set Design

The training data set is generated by running 24 10-day GFS forecasts, configured as described above, initialized at 00Z on the 1st and the 15th of each month of 2018 with instantaneous data saved three-hourly to capture diurnal and annual cycles (see below what specifically is being saved). Note, that in GFS both the dynamical core and the full physics package operate on a globally quasi-uniform cubed sphere grid, while, for the sake of compatibility with other components of the forecasting system (e.g. DA, post-processing), the output of the model is saved on a full Gaussian grid that has resolution at the equator comparable to that of the native grid, but a higher resolution closer to the poles. Therefore, the number of columns on a given latitude that are included in the training set is selected to be proportional to the cosine of the latitude in order to avoid over-representation of the polar areas in the training set. First 23 of the 24 runs that produced 141,557,760 profiles in total were used to create the trainig and test sets. The last run, initialized on 0Z of December 15, 2018, was used to create an independent validation set and to perform an independent parallel run.

After taking into account latitudinal dependence, less than 1% of profiles were randomly selected from each 3-hourly global field. As a result, three independent data sets have been created: 1) training set containing 414,000 records, 2) test set containing 414,000 records, and 3) validation set containing 250,000 records.

3.2. NN Architecture

A "shallow" NN, the multilayer perceptron NN with one hidden layer, was used in this study:

$$y_j = b_j^1 + \sum_{i=1}^{k} a_{ji}^1 \cdot t_i \ , \ \ j = 1, \cdots, M$$

$$t_i = \phi(b_i^0 + \textstyle\sum_{s=1}^{N} a_{is}^0 \cdot \ x_s), \ \ s = 1, \cdots, N \qquad (1)$$

Here a and b are NN weights and biases, and N, k, and M are numbers of NN inputs, hidden neurons, and outputs correspondingly.

The reason for choosing this type of NN is twofold. First, model physics is a continuous or almost continuous mapping, and shallow NN is a generic analytical nonlinear approximation or model for such a mapping [30] that, from a theoretical standpoint, guarantees that a mathematical solution of the machine learning problem exists [31]. Second, our experience with using shallow NNs for emulating complex multidimensional mappings [32] shows that shallow NNs can provide accurate emulations of mappings, and demonstrate very high stability in the long term model integration, as well as robustness with respect to substantial structural and parametric change in their host model [33].

A shallow NN with 506 inputs, 304 outputs, and 250 hidden neurons in the hidden layer was trained using a back-propagation algorithm with adjustable learning rate and other hyper-parameters, as well as with multiple exit conditions.

Table 1 Full NN Model Physics Suite Inputs and Outputs

NN Input	NN Input #	Layers	NN Input	NN Input #	Layers
$\cos\frac{2\cdot\pi\times day}{366}$	1	-	Surface Pressure	137	-
$\sin\frac{2\cdot\pi\times day}{366}$	2	-	U-wind	138 : 201	1 : 64
$\cos\frac{2\cdot\pi\times month}{366}$	3	-	V-wind	202 : 265	1 : 64
$\sin\frac{2\cdot\pi\times month}{366}$	4	-	Vertical velocity	266 : 329	1 : 64
Latitude	5	-	Temperature	330 : 393	1 : 64
cos(*Longitude*)	6	-	Specific humidity	394 : 430	1 : 37
sin(*Longitude*)	7	-	Total cond. mix. ratio	431 : 473	1 : 43
cos(*Zenith Angle*)	8	-	Ozone mixing ratio	474 : 505	33 : 64
Layer geop. height	9 : 72	1 : 64	Solar constant	506	-
Layer pressure	73 : 136	1 : 64			
NN Output	NN Output #	Layers	NN Output	NN Output #	Layers
U-wind increment	1 : 64	1 : 64	Specic humidity incr.	193 : 229	1: 37
V-wind increment	65 : 128	1 : 64	Total cond. m. r. incr.	230 : 272	1 : 43
Temperature incr.	129 : 192	1 : 64	Ozone mixing ratio incr.	273 : 304	33 : 64

Table 1 shows inputs and outputs of the NN model physics suite (NMPS). Some input variables have zero values on the upper (e.g. water vapor) or the lower (e.g. ozone) vertical layers. Constant inputs (zero or nonzero) do not contribute to the functional input/output relationship of the approximated mapping and were removed. To correctly emulate the response of the physics package to a given set of atmospheric state variables generated by the dynamical core, the NN must be supplied with the information on the Solar energy input into the current atmospheric column, composition of the atmosphere in it, along with other information the dynamical core does not provide. More specifically, to capture the effects of temporal and spatial variability of greenhouse gases and aerosols, we note that in GFS greenhouse gas and aerosol concentrations are given by climatologically derived look-up tables that vary with month of the year and the location on the globe; therefore, we supply the NN with the geographical location of a given column and a periodic function of the current month number. Position of said column on the globe with respect to the Sun

is represented by the cosine of solar zenith angle input to the NN. Location of Earth in orbit is captured by periodic functions of day and month number. Variability of solar radiation is captured by the solar "constant" input to the NN. All NN outputs are increments of dynamical core's prognostic variables that the original MPS modifies. These modified variables are returned to the dynamical core.

4. Coupling of Full Model Physics NN to GFS

Replacement of MPS with NMPS in GFS results in a new model, which will be referred to as a hybrid GFS (HGFS). In this pilot study, the NN is configured to update the state of the atmosphere (the six prognostic variables mentioned in Section 2), but, unlike the original physics package, it produces neither the diagnostic output of GFS nor the land surface model related output. In addition, GFS calculates astronomy-related parameters inside the physics package. Therefore, to ensure that HGFS produces the same diagnostic output as GFS, and that solar-related inputs to the NN are updated correctly, we couple the NFMS to GFS in a manner illustrated on Figure 1 and described below.

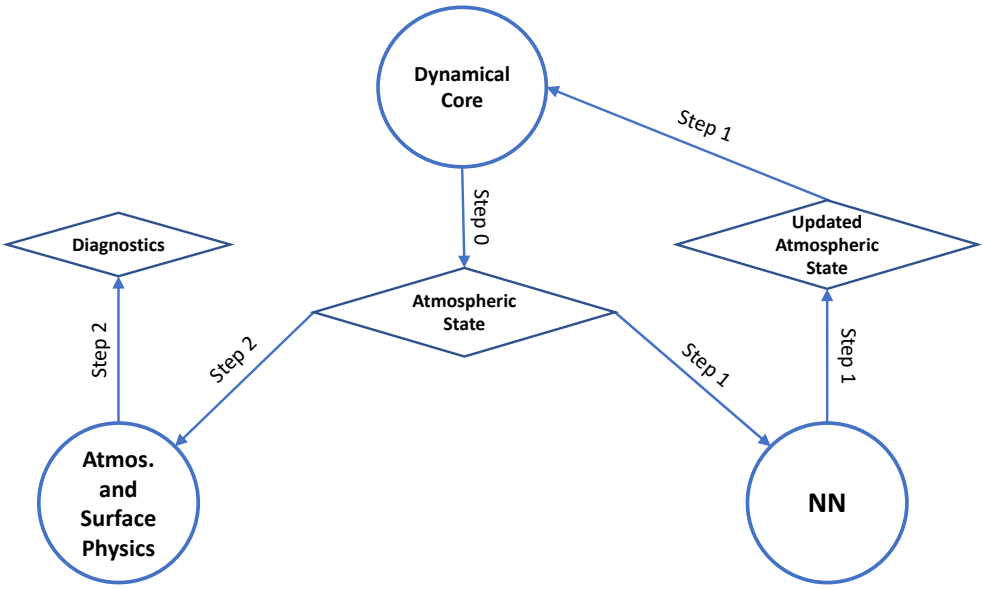

Figure 1. Coupling of the NN model physics to GFS. Step 2 may be performed significantly less frequently than Step 1 that is performed at each time step.

At each time step, the updated atmospheric state from the dynamical core is supplied to both the NMFS and the original MPS. NMPS is called to calculate an update to the atmospheric state. Atmospheric state is then modified by the update from the NMPS and is returned to the dynamical core to be used on the next time step. Original physics suite is ran after that to produce GFS diagnostics and to update solar-related variables.

5. Validation of NN MPS in Parallel Runs of GFS and HGFS

In the following we will concentrate on analysis of variables directly modified by the neural network, or prognostic variables of the atmospheric dynamical core, as opposed to the output of the diagnostic package. Analysis of the latter along with evaluation of the NN's impact on forecast quality will be presented in a later publication.

We performed 23 10-day HGFS forecasts using the same initial conditions that were utilized in generation of the training data set, as well as an additional 10-day HGFS forecast using the initial

conditions utilized in generation of the independent validation set. All 24 forecasts carried out with the NN replacing the original physics package were stable. It's worth noting that even though initial conditions for the first 23 runs are the same as the ones used for generation of the NN training sets, only less than 1% of all atmospheric states saved during creation of this data set were used in NN training. Moreover, internally, GFS updates the atmospheric state and, consequently, invokes the NN much more frequently than the 3-hourly output cadence used in generation of the training set. For example, at C96L64 resolution the NN is called every 450 model seconds. As a result, the NMPS is almost exclusively exposed to the inputs that were not present or used in training.

Figures 2 and 3 show zonal and time means of an average over 24 10-day forecasts produced by HGFS (top panels), and by GFS configured as described in Section 2 (middle panels). The bottom panels show the differences/biases between the NN and the control runs. Vertical coordinate shows model level number. All variables predicted by the NN compare well to the control. Global time averaged biases are on the order of 1% or less for meridional component of wind and total cloud condensate; for all other variables these biases are on the order of 0.01% or smaller. Local biases can be larger in magnitude than global biases. Zonal wind, U, shown in the left column of Figure 3, exhibits upper tropospheric biases of about 0.1 m/s that are cold in midlatitudes and warm in the subtopics. This pattern is consistent with the equatorward shift of the subtropical jets. However, these biases are only about 1% of the local absolute magnitude of U. Temperature, T, shown in the right column of Figure 3, has warm biases of about 0.05 K throughout polar troposphere, and cold biases of approximately -0.1 K in the polar tropopause. These biases extend further away from the pole in the Southern Hemisphere than in the Northern Hemisphere. Nevertheless, local T biases at their largest are less than 0,01 % of the local temperature values. Ozone, O_3, shown on the right panel of Figure 4, exhibits mostly positive polar stratospheric biases that are less than 1% of the local ozone concentrations. There's also a smaller positive O_3 bias throughout the upper stratosphere.

We also examine temporal evolution of global biases. Figure 4 shows time evolution of zonal and vertical means of global biases averaged over 24 10-day forecasts. Notably, this perspective suggests that all local biases discussed in the previous paragraph develop after day 7 of the forecast, except the polar temperature bias that is present from day one. However, there's more nuance to this picture. Figure 5 shows time evolution of zonal and meridional mean vertical profile of global biases averaged over 24 10-day forecasts. Small positive upper stratospheric O_3 bias is present from the beginning of the forecast. There's a cold T bias in the upper stratosphere and a warm bias in the upper troposphere that are strongest in the beginning of the forecast but decrease as time progresses. There's also a positive upper tropospheric total cloud condensate bias in the first day of the forecast. Once again, all of these biases (differences between NN and control runs) are small.

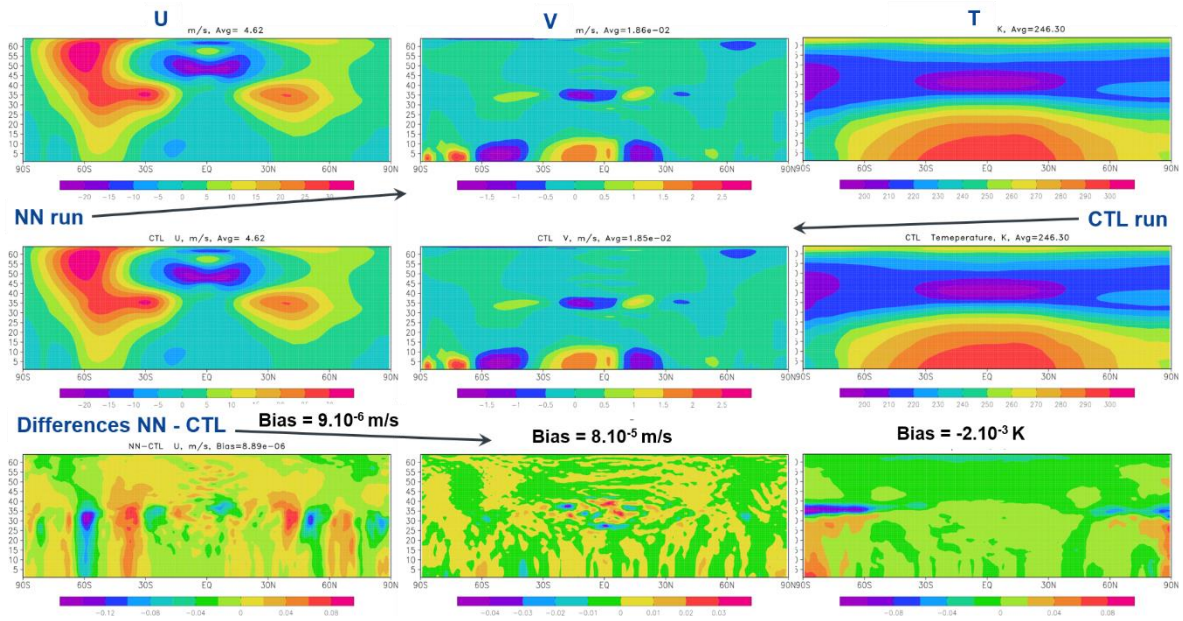

Figure 2. Zonal and time means of an overage over 24 10-day forecasts for U (left column), V (central column), and temperature (right column). Upper row – results produced by HGFS, medium – by GFS, and the lower row the difference (HGFS – GFS). Vertical coordinate shows model level number.

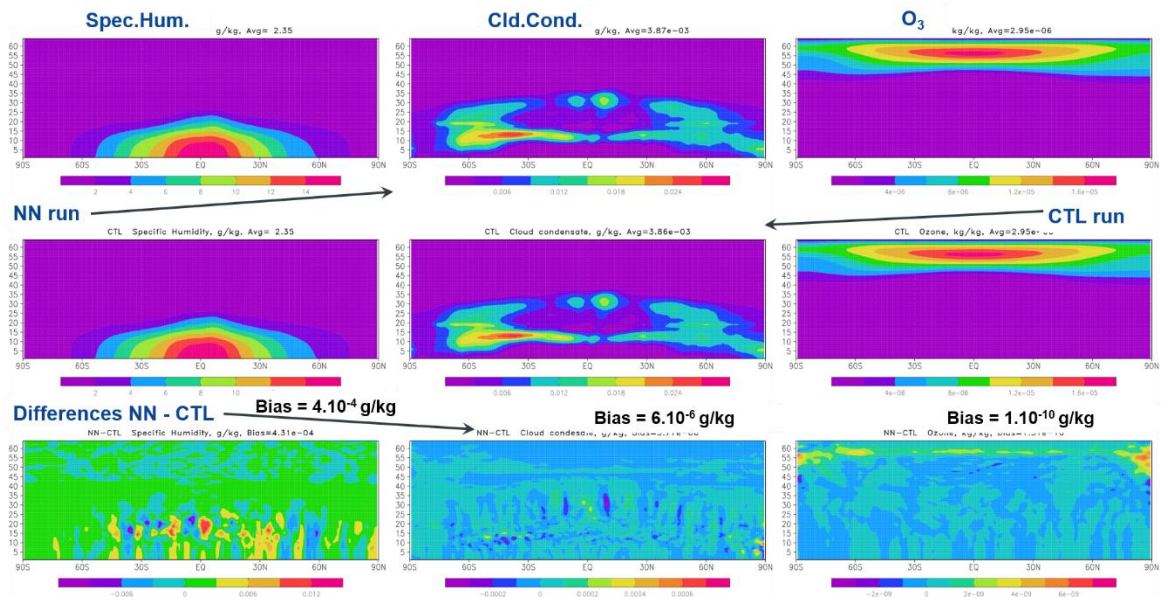

Figure 3. Zonal and time means of an overage over 24 10-day forecasts for specific humidity (left column), total cloud condensate (central column), and ozone mixing ratio (right column). Upper row – results produced by HGFS, medium – by GFS, and the lower row the difference (HGFS – GFS). Vertical coordinate shows model level number.

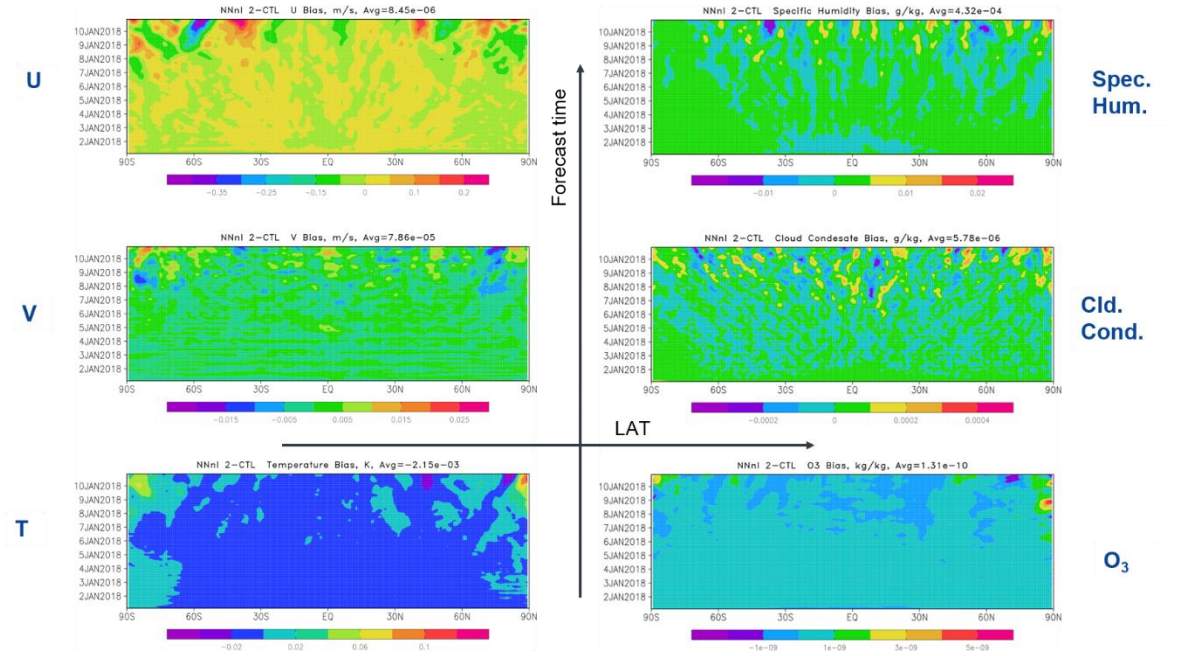

Figure 4. Time evolution of zonal and vertical means of global biases averaged over 24 10-day forecasts for U (upper right), V (central right), temperature (lower right), specific humidity (upper left), cloud condensate (central left) and ozone mixing ratio (lower left).

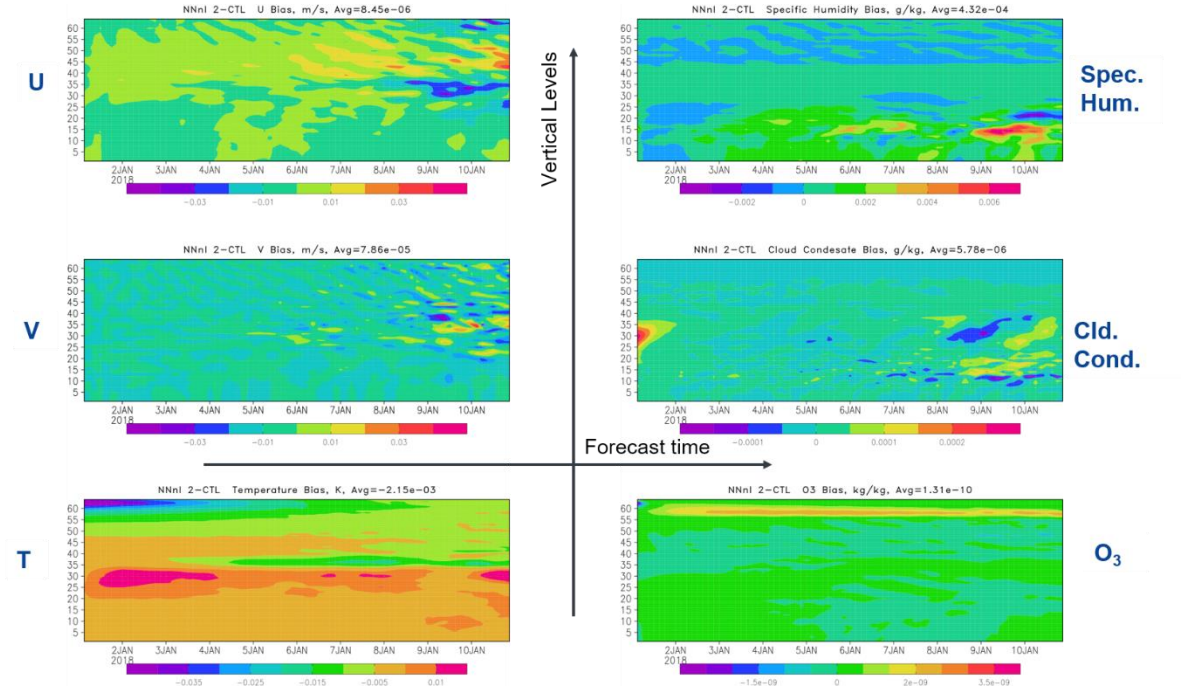

Figure 5. Time evolution of zonal and meridional mean vertical profile of global biases averaged over 24 10-day forecasts for U (upper right), V (central right), temperature (lower right), specific humidity (upper left), total cloud condensate (central left) and ozone mixing ratio (lower left). Vertical coordinate shows model level number.

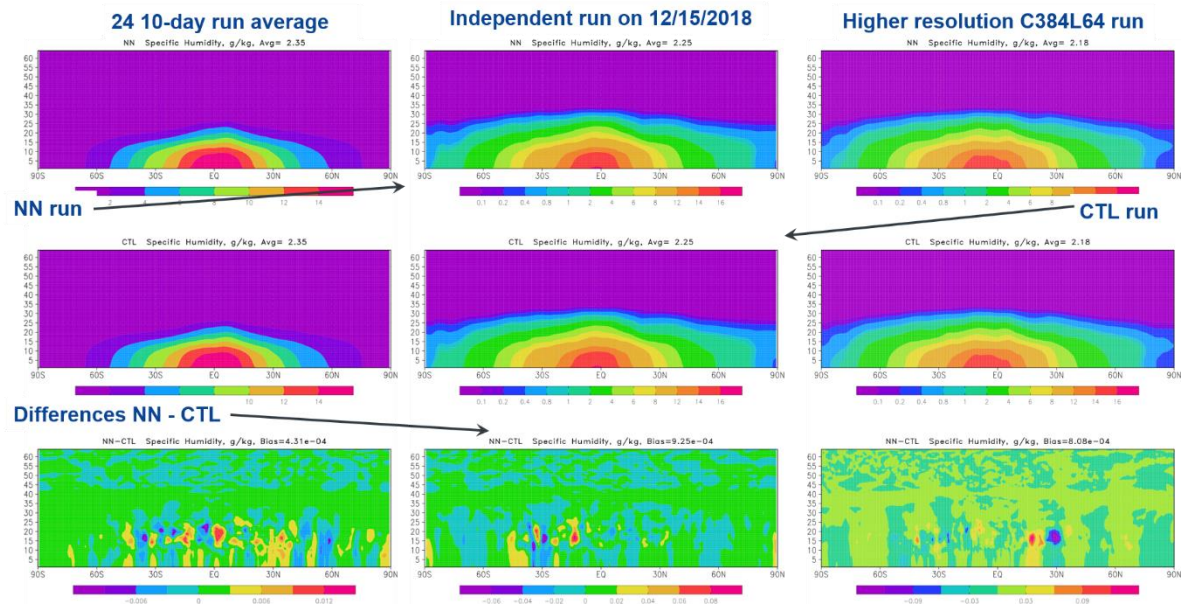

Figure 6. Time and zonal means of specific humidity. Average over 24 10-day forecasts (left column), average over an independent10-day forecast initialized on December 15, 2018 (central column), and a high resolution (C384, ~25 km) run (right column) initialized on January 1, 2018. NN run (upper row), control run (central row), the difference NN – control (lower row). Vertical coordinate shows model level number.

To test stability of the developed NMPS in longer experiments, a one model year long continuous AMIP-like run was successfully performed. The NN was stable during the integration. In addition, to evaluate the robustness of NMPS with respect to changes in the model configuration, we performed a run with a higher horizontal resolution of C384 (~25 km). It is four times as high as the model resolution used during the generation of data for training (~100 km). Vertical resolution, L64, was kept the same. The comparison of the specific humidity fields (left column) averaged over 24 10-day C96L64 forecasts initialized on 0Z of the 1st and the 15th of each month of 2018, (central column) averaged over a single independent 10-day C96L64 forecast initialized on 0Z of 12/15/18, and (right column) averaged over a 10-day C384L64 forecast initialized on 0Z of 1/1/18, are presented on Figure 6. The structure and magnitude of biases is generally similar between all three experiments, with small random biases generally located in the tropical mid-troposphere.

NN-based emulation of the entire GFS model physics suite is three times as fast as the original physics block configured to calculate radiation with the same frequency as the rest of model physics. However, optimization of the NN architecture will provide additional speedup.

6. Conclusions

A shallow NN based emulator of an entire suite of atmospheric physics parameterizations in a state-of-the-art GCM has been developed. NCEP GFS with the neural network replacing the original suite of atmospheric parameterizations produces stable and realistic medium range weather forecasts for 24 initial conditions spanning all months of 2018. It also remains stable in a year-long AMIP-like experiment and in a 10-day forecast with quadrupled horizontal resolution. The emulator is three times as fast as the original suite of physics parameterizations.

Many centers such as NCEP [34], ECMWF [35] and the UK Met Office [36] use 4D-Var data assimilation The success of the 4D-Var approach is crucially dependent on the construction of accurate tangent-linear and adjoint versions of every model component, especially for the physical parametrization schemes that represent the unresolved part of the model physics. Constructing these linearized models can either be achieved by manually differentiating the nonlinear code or by using

an automatic differentiation tool [37]. The NN emulation presented in this paper represents the entire suite of the model physics (including a land model). It is easily differentiable and can serve as a basis for building fast adjoint for entire suite of model physics without calculation multiple linearized models for each constituent of the model physics suite.

Potential next steps for our project are: 1) optimize NN architecture to increase speedup provided by NMPS , 2) perform cycled experiments with data assimilation to verify HGFS against its own analysis and to fully assess forecast errors, 3) include GFS diagnostics in NMPS outputs to eliminate need in calling MPS to calculate diagnostics and to completely use the speedup provided by NMPS, 4) if found necessary, generate a new version of training data set saved directly on the GFS's native cubed sphere grid.

Author Contributions: Conceptualization, A.B. and V.K.; methodology, A.B. and V.K.; data for training, A.B.; NN training V.K.; NN validation, A.B.; analysis of results A.B. and V.K.; writing A.B. and V.K. All authors have read and agreed to the published version of the manuscript.

Funding: This research was supported by grant number EA133W-17-CN-0016 supported by NOAA Weather Program Office Joint Technology Transfer Initiative.

Acknowledgments: The authors would like to thank Drs. Ruiyu Sun and Jun Wang for valuable help with practical use of NCEP GFS and for useful discussions and consultations. We also thank Drs. Jack Kain, Fanglin Yang, and Vijay Tallapragada for their support.

Conflicts of Interest: The authors declare no conflict of interest.

References

1. Chevallier, F.; Morcrette, J.-J.; Chéruy, F.; Scott, N. A. Use of a neural-network-based longwave radiative transfer scheme in the ECMWF atmospheric model. *Quarterly Journal of the Royal Meteorological Society*, 2000, 126, 761-776
2. Krasnopolsky, V.; Chalikov, D.; Tolman, H. L. A neural network technique to improve computational efficiency of numerical oceanic models. *Ocean Modelling*, 2002, 4, 363-383
3. Krasnopolsky, V. M.; Fox-Rabinovitz, M. S.; Chalikov, D. V. New Approach to Calculation of Atmospheric Model Physics: Accurate and Fast Neural Network Emulation of Long Wave Radiation in a Climate Model. *Monthly Weather Review*, 2005, 133, 1370-1383
4. Krasnopolsky, V. M.; Fox-Rabinovitz, M. S.; Hou, Y. T.; Lord, S. J.; Belochitski, A. A. Accurate and Fast Neural Network Emulations of Model Radiation for the NCEP Coupled Climate Forecast System: Climate Simulations and Seasonal Predictions, *Monthly Weather Review*, 2010, 138, 1822-1842. doi: 10.1175/2009MWR3149.1
5. Krasnopolsky, V.; Belochitski, A. A.; Hou, Y.-T.; Lord S.; Yang F. Accurate and fast neural network emulations of long and short-wave radiation for the NCEP Global Forecast System model. 2012, *NCEP Office Note 471*, Camp Springs, MD. https://repository.library.noaa.gov/view/noaa/6951
6. Pal, A.; Mahajan, S.; Norman, M. R. Using deep neural networks as cost-effective surrogate models for Super-Parameterized E3SM radiative transfer. *Geophysical Research Letters*, 2019, 46, 6069–6079. https://doi.org/10.1029/2018GL081646
7. Mooers, G.; Pritchard M.; Beucler T.; Ott, J.; Yacalis, G.; Baldi, P.; Gentine, P. Assessing the Potential of Deep Learning for Emulating Cloud Superparameterization in Climate Models with Real-Geography Boundary Conditions. arXiv:2010.12996v1 [physics.ao-ph] 24 Oct 2020
8. Krasnopolsky, V. M., Fox-Rabinovitz, M. S., Rasch, P. J., Wang, M. Fast NN Emulation of the Super-Parameterization in the Multi-scale Modeling Framework, 2014, *NCEP Office Note 476*, https://www.lib.ncep.noaa.gov/ncepofficenotes/files/on476.pdf
9. Gentine, P.; Pritchard, M.; Rasp, S.; Reinaudi, G.; Yacalis G. Could machine learning break the convection parameterization deadlock? *Geophysical Research Letters*, 2018,45, 5742–5751.
10. Krasnopolsky, V. M.; Fox-Rabinovitz, M. S.; Belochitski, A. A. Using Ensemble of Neural Networks to Learn Stochastic Convection Parameterization for Climate and Numerical Weather Prediction Models from Data Simulated by Cloud Resolving Model. *Advances in Artificial Neural Systems*, 2013, Article ID 485913, 13 pages. doi:10.1155/2013/485913

11. Brenowitz, N. D.; Bretherton C. S. Spatially extended tests of a neural network parametrization trained by coarse-graining. *Journal of Advances in Modeling Earth Systems*, 2019, 11, 2728–2744.
12. Beucler T.; Pritchard M.; Gentine P.; Rasp S. Towards Physically-consistent, Data-driven Models of Convection. 2020, arXiv:2002.08525 [physics.ao-ph]
13. Krasnopolsky, V.; Lord S.; Moorthi S.; Spindler T. How to deal with inhomogeneous outputs and high dimensionality of neural network emulations of model physics in numerical climate and weather prediction models. Proceedings of International Joint Conference on Neural Networks, 2009, Atlanta, GA, 1668–1673.
14. Harris, L. M. and S.-J. Lin: 2013, A two-way nested global-regional dynamical core on the cubed-sphere grid. Monthly Weather Review, 141, 283–306.
15. Putman, W. and S.-J. Lin: 2007, Finite-volume transport on various cubed-sphere grids. Journal of Computational Physics, 227, 55–78.
16. Kain, J. S.; Moorthi, S.; Yang, F.; Yang, R.; Wei, H.; Wu, Y.; Hou, Y.-T.; Lin, H.-M.; Yudin, V. A.; Alpert, J. C.; Tallapragada, V.; Sun R. Advances in model physics for the next implementation of the GFS (GFSv16). AMS Annual Meeting, Boston, 2020, MA, 6A.3.
17. Mlawer, E. J., S. J. Taubman, P. D. Brown, M. J. Iacono, and S. A. Clough: 1997, Radiative transfer for inhomogeneous atmospheres: RRTM, a validated correlated-k model for the longwave. Journal of Geophysical Research: Atmospheres, 102, 16663–16682.
18. Clough, S., M. Shephard, E. Mlawer, J. Delamere, M. Iacono, K. Cady-Pereira, S. Boukabara, and P. Brown: 2005, Atmospheric radiative transfer modeling: a summary of the AER codes. Journal of Quantitative Spectroscopy and Radiative Transfer, 91, 233 – 244.
19. Han, J.; Bretherton, C. S. TKE-based moist eddy-diffusivity mass-flux (EDMF) parameterization for vertical turbulent mixing. Weather and Forecasting, 2019, 34, 869–886.
20. Lott, F. and Miller, M.J. (1997), A new subgrid-scale orographic drag parametrization: Its formulation and testing. Q.J.R. Meteorol. Soc., 123: 101-127
21. Yudin, V, F. Yang, S Karol, T. Fuller-Rowell, A. Kubaryk, H. Juang, S. Kar,J. Alpert, Z. Li: 2020, The Unified Gravity Wave Physics in the Vertically Extended Atmosphere Models of NGGPS and UFS, UFS User's Workshop, July 27-29 2020
22. Pan, H.-L. and W.-S. Wu: 1996, Implementing a mass flux convective parameterization package for the NMC medium-range forecast model. NCEP Office Note, 409, 40 pp.
23. Han, J. and H.-L. Pan: 2011, Revision of convection and vertical diffusion schemes in the NCEP global forecast system. Weather and Forecasting, 26, 520–533.
24. Han, J.; Pan H.-L. Revision of convection and vertical diffusion schemes in the NCEP Global Forecast System. Weather and Forecasting, 2011, 26, 520–533.
25. Han, J.; Wang W.; Kwon, Y. C.; Hong, S.-Y.; Tallapragada, V.; Yang F. Updates in the NCEP GFS cumulus convection schemes with scale and aerosol awareness. Weather and Forecasting, 2017, 32, 2005–2017
26. Lin, Y.-L.; Farley, R. D.; Orville, H. D. Bulk parameterization of the snow field in a cloud model. *Journal of Climate and Applied Meteorology*, 1983, 22, 1065–1092.
27. Chen, J.-H.; Lin S.-J. The remarkable predictability of inter-annual variability of Atlantic hurricanes during the past decade. *Geophysical Research Letters*, 2011, 38, L11804, doi:10.1029/2011GL047629.
28. Ek, M. B., K. E. Mitchell, Y. Lin, E. Rogers, P. Grunmann, V. Koren, G. Gayno, and J. D. Tarpley: 2003, Implementation of noah land surface model advances in the national centers for environmental prediction operational mesoscale eta model. Journal of Geophysical Research: Atmospheres, 108.
29. Zhao, Q.; Carr F. H. A Prognostic Cloud Scheme for Operational NWP Models. *Monthly Weather Review*, 1997, 125, 1931–1953.
30. Hornik, K. Approximation Capabilities of Multilayer Feedforward Network. *Neural Networks*, 1991, 4, 251-257
31. Vapnik, V. N. Complete Statistical Theory of Learning, *Automation and Remote Control*, 2019, 80 (11), 1949–1975.
32. Krasnopolsky, V. *The Application of Neural Networks in the Earth System Sciences. Neural Network Emulations for Complex Multidimensional Mappings*. Atmospheric and Oceanic Science Library. (Vol. 46). Dordrecht, Heidelberg, New York, London: Springer, 2013; 200pp.; DOI 10.1007/978-94-007-6073-8
33. Belochitski, A.A.; Krasnopolsky, V. Robustness of NN Emulations of Radiative Transfer Parameterizations in a State-of-the-Art General Circulation Model. This issue.

34. Kleist, D. T., & Ide, K. (2015). An OSSE-Based Evaluation of Hybrid Variational–Ensemble Data Assimilation for the NCEP GFS. Part II: 4DEnVar and Hybrid Variants, Monthly Weather Review, 143(2), 452-470.
35. Bauer, P., Quintino, T., Wedi, N., Bonanni, A., Chrust, M., Deconinck, W., Zanna, C. (2020). The ECMWF Scalability Programme: Progress and Plans (Tech. Rep.). doi: 10.21957/gdit22ulm
36. Payne, T. J. (2021). A Hybrid Differential-Ensemble Linear Forecast Model for 4D-Var. *Monthly Weather Review*, 149 (1), 3–19.https://doi.org/10.1175/MWR-D-20-0088.1
37. Hatfield, S., M. Chantry, P. Dueben, P. Lopez, A. Geer, T. Palmer (2021*). Journal of Advances in Modeling Earth Systems,* in press.